第 31 卷 第 5 期 高 能 物 理 与 核 物 理 Vol. 31, No. 5
2007 年 5 月 HIGH ENERGY PHYSICS AND NUCLEAR PHYSICS May, 2007

Effect of the Incident Energy on the Observables of Proton Elastic Scattering on Halo Nucleus*

GU Bai-Ping[1,2;1)] MAO Ying-Chen[1]

1 (Department of Physics, Nanjing University, Nanjing 210008, China)
2 (Department of Mathematics and Physics, Nanjing University of TCM, Nanjing 210029, China)

Abstract The proton elastic scatterings on ^{14}Be, ^{16}O and ^{12}C at the intermediate incident energies of 200, 400 and 800MeV, are investigated within the relativistic impulse approximation (RIA). The effect of the incident energy on three observables, the differential cross section, the analyzing power and the spin rotation function, is discussed. It is shown that in the region of small scattering angle, the halo neutron effect on the observables exhibits an unchanged tendency with the variation of the incident energy of proton in the intermediate energy region.

Key words proton elastic scattering, relativistic impulse approximation (RIA), halo nuclei, differential cross section, analyzing power, spin rotation function

1 Introduction

For decades, the study of exotic nuclei that are near the drip lines on N-P plane has drawn great attention of nuclear physicists around the world[1]. Halo nucleus is one kind of such nuclei, whose properties have been studied ever since Tanihata and his coworker's work in 1985[2]. Near the neutron drip line, the low neutron binding energy makes the wave function of the peripheral neutrons extend far beyond the range of the strong force. This gives rise to the neutron halo phenomenon, which has already been observed in some light nuclei such as ^{11}Li, ^{14}Be, ^{6}He and ^{8}He, etc.[3—13]. Near the proton drip line, the proton-rich nuclei, such as ^{8}B, ^{17}F, ^{17}Ne, ^{23}Al and $^{26-28}$P, show some proton halo structures[14—19]. Halo nuclei could be detected by a variety of experimental methods[20, 21], such as the beta-decay measurement following in-beam polarization and the investigation of the momentum distributions of reaction products produced in bombarding a nuclear target with a halo nucleus[9]. As is known to all, the elastic proton scattering on nuclei at intermediate energies could provide important information of the nucleon-nucleon (NN) interaction, the radial structure of the target nucleus and reaction mechanisms[10, 22, 23]. The differential cross section $\mathrm{d}\sigma/\mathrm{d}\Omega$, the analyzing power A_y and the spin rotation function Q are three important observables in describing proton elastic scattering on target. The relativistic impulse approximation (RIA)[24—27] is one of the useful schemes to describe proton elastic scattering off nuclei at intermediate incident energies between 100 and 1000MeV, microscopically. Murdock and Horowitz[28] calculated the obsevables for proton elastic scattering off ^{12}C, ^{16}O, ^{40}Ca and ^{208}Pb around 200MeV and reproduced the data remarkably well within the RIA formalism. Ray[29] combined RIA with the distorted wave Born

Received 2 August 2006, Revised 29 January 2007
* Supported by National Natural Science Foundation of China (10535010, 10125521), Major State Basic Research Development Program of China (G2000077400), Knowledge Innovation Project of CAS (KJCX2-SW-N02) and Doctoral Fund of Ministry of Education of China (20010284036)
1) E-mail: medphystcm@126.com

approximation (DWBA) and used the RIA-DWBA scheme to study proton elastic scattering on nuclei with non-zero-spin. Sakaguchi et al[30] employed RIA to analyze the elastic scattering data of the p-^{58}Ni process at the incident energies of 192, 295 and 400MeV, respectively. Recently, Baldini-Neto et al[31] extended the RIA scheme to describe proton elastic scattering off exotic nuclei such as the p-^{6}He and p-^{8}He processes. In the present paper, by using the RIA formalism, we study the elastic scatterings in the p-^{14}Be, p-^{16}O and p-^{12}C processes at $E_{\rm lab}$=200, 400 and 800MeV, respectively, and compare the resultant $\mathrm{d}\sigma/\mathrm{d}\Omega$, A_y and Q for these processes at each energy. We find that excessive neutrons in ^{14}Be most probably affect $\mathrm{d}\sigma/\mathrm{d}\Omega$, A_y and Q at the small scattering angles, and the affected angular range is narrowed as the projectile energy increases. These phenomena may help us to understand some of the properties of the neutron-riched nuclei.

2 The theoretical formalism

In RIA, the NN scattering operator, denoted as $\Im(q,E;n)$[32, 33], is represented by a set of Lorentz invariants

$$\Im(q,E;n)=\sum_{\rm L}\Im^{\rm L}(q,E;n)\lambda^{\rm L}_{(0)}\cdot\lambda^{\rm L}_{(n)}\ , \tag{1}$$

where $\lambda^{\rm L}_{(i)}$ stands for the Dirac operator (or Dirac matrix[28]) for the incident nucleon ($i=0$) and struck nucleon ($i=n$ with n being the n-th nucleon in the target nucleus), the dot product implies that all the Lorentz indices are contracted, L stands for the scalar (S), vector (V), pseudoscalar (PS), tensor (T), axial vector (A) fields, respectively. $\Im^{\rm L}(q;E)$ is a complex function of momentum transfer q and laboratory energy E.

If applying this approximation to the proton elastic scattering off a spherical nucleus, the first order Dirac optical potential which deals with single-scattering approximation and spin-saturated nucleus, contains only the scalar and vector potentials, and can be written as

$$U_{\rm opt}=U^{\rm S}+\gamma^0U^{\rm V}\ , \tag{2}$$

$$U^{\rm L}=U^{\rm L}_{\rm D}(r;E)+U^{\rm L}_{\rm X}(r;E)\ , \tag{3}$$

where γ^0 is the gamma matrix[34],

$$U^{\rm L}_{\rm D}(r;E)\ =\ -\frac{4\pi{\rm i}p}{M}\int{\rm d}^3x'\rho^{\rm L}(\boldsymbol{x}')t^{\rm L}_{\rm D}(|\boldsymbol{x}-\boldsymbol{x}'|;E)\ , \tag{4}$$

$$U^{\rm L}_{\rm X}(r;E)\ =\ -\frac{4\pi{\rm i}p}{M}\int{\rm d}^3x'\rho^{\rm L}(\boldsymbol{x},\boldsymbol{x}')t^{\rm L}_{\rm X}(|\boldsymbol{x}-\boldsymbol{x}'|;E)\times j_0(p|\boldsymbol{x}-\boldsymbol{x}'|)\ , \tag{5}$$

are direct and exchange optical potentials, respectively, with j_0 being the zeroth order spherical Bessel function, and $t^{\rm L}(|\boldsymbol{x}|,E)$ functions having the forms as those in Refs. [27—29]. The densities in Eqs. (4) and (5) can be expressed as

$$\rho^{\rm L}(\boldsymbol{x}',\boldsymbol{x})\ =\ \sum_{\kappa}^{\rm occupied}\bar{u}_\kappa(x')\lambda^{\rm L}u_\kappa(x)\ , \tag{6}$$

$$\rho^{\rm L}(\boldsymbol{x})\ \equiv\ \rho^{\rm L}(\boldsymbol{x},\boldsymbol{x})\ , \tag{7}$$

where u_κ is the single-particle wave function, κ runs over all the occupied states of the target nucleus. The off-diagonal one-body density is approximated by the local-density[35]

$$\rho^{\rm L}(\boldsymbol{x}',\boldsymbol{x})\approx\rho^{\rm L}\left(\frac{1}{2}(\boldsymbol{x}'+\boldsymbol{x})\right)\left(\frac{3}{sk_{\rm F}}\right)j_1(sk_{\rm F}), \tag{8}$$

where $s\equiv|\boldsymbol{x}'-\boldsymbol{x}|$ and $k_{\rm F}$ is related to the nuclear baryon density by $\rho_{\rm B}\left(\frac{1}{2}(\boldsymbol{x}'+\boldsymbol{x})\right)=\frac{2k^3_{\rm F}}{3\pi^2}$, j_1 denotes the first order spherical Bessel function.

For intermediate incident energies, it is necessary to correct the optical potentials with the Pauli blocking effect,

$$U^{\rm L}(r;E)\rightarrow\left[1-a(E)\left(\frac{\rho_{\rm B}(r)}{\rho_0}\right)^{2/3}\right]U^{\rm L}(r;E), \tag{9}$$

where $\rho_{\rm B}(r)$ is the local baryon density of the target with ρ_0=0.1934fm^{-3}, and $a(E)$ the “Pauli blocking factor”[28]. All the above densities are calculated by using the relativistic mean field theory (RMF)[36—38] and then are applied to calculate Dirac optical potentials with the equations discussed above.

The Dirac equation for the projectile is then written as

$$\left[-{\rm i}\boldsymbol{\alpha}\cdot\nabla+U^{\rm V}(r;E)+\beta(M+U^{\rm S}(r;E))\right]|\psi\rangle=E\,|\psi\rangle\ , \tag{10}$$

where M is the rest mass of the projectile, E the projectile energy in the center of mass (c.m.) frame. By selecting correct asymptotic boundary conditions, we can solve Eq. (10) numerically and consequently obtain the results of the observables $\mathrm{d}\sigma/\mathrm{d}\Omega$, A_y and Q, respectively, in the elastic proton scattering process.

3 The results and discussions

By using the RIA formalism, we obtain $\mathrm{d}\sigma/\mathrm{d}\Omega$, A_y and Q for the proton elastic scattering off the nuclei ^{14}Be, ^{16}O and ^{12}C, respectively. As the Dirac optical potentials U^{L} which are given in Eqs. (4), (5) and (9) contain the densities of scalar and vector fields, we firstly have to calculate the proton and neutron density distributions of target nuclei ^{14}Be, ^{16}O and ^{12}C, respectively, based on the RMF theory with the parameter set NL3[33]. The binding energy is adjusted by the center of mass correction with the HS scheme for light nuclei[33]. The density distributions of the target nucleus and the Dirac optical potentials U^{L} for the proton elastic scattering off above three nuclei at E_{lab}=200MeV have been presented in Ref. [33]. In the present work, Dirac optical potentials for the same scattering systems at E_{lab}=800MeV are calculated and plotted in Fig. 1. It is shown that the Dirac optical potentials for the p-^{14}Be system, in comparison with other two systems, exhibit the same ‘long-tail’ phenomenon as that in Ref. [33] at E_{lab}=200MeV. This kind of ‘long-tail’ in Fig. 1 is considered as the result of the extended neutron distribution in the halo nucleus ^{14}Be. In Table 1 some resultant quantities in the RMF theory and the corresponding data, which characterize nuclear properties, are tabulated. It is shown that the RMF results (marked by Theo.), such as the average binding energy[39], rms radius[40] and the rms charge radius[41], agree with the experimental data (marked by Expt.) very well. In the columns for ^{14}Be(Expt.), the rms charge radius of ^{14}Be is obtained by the empirical formula $R_{\mathrm{e}} = r_{\mathrm{e}}A^{\mathrm{e}}$, where $r_{\mathrm{e}} = 1.153(7)$ and $e = 0.2938(12)$[41]. Finally, the observables $\mathrm{d}\sigma/\mathrm{d}\Omega$, A_y and Q for the elastic scatterings of p-^{14}Be, p-^{16}O and p-^{12}C at E_{lab}=200, 400 and 800MeV are evaluated, respectively. The results are demonstrated in Figs. 2—4, respectively, where $\theta_{\mathrm{c.m.}}$ is the scattering angle in the c.m. frame, σ stands for $\mathrm{d}\sigma/\mathrm{d}\Omega$ in the present work and σ_{M} denotes the Mott cross section[42]. In order to check the validity of RIA in describing the proton elastic scattering on the nucleus at the intermediate energy, we calculate the elastic scattering for p-^{12}C and p-^{16}O at E_{lab}=200MeV, respectively. The theoretical results and the data are illustrated in Fig. 5 and Fig. 6, respectively. From Fig. 5 and Fig. 6, one sees that the RIA results at E_{lab}=200MeV are in good agreement with the data especially in the small angular regions. Other proofs can also be found in literatures[25—28, 30—32]. Therefore, RIA is a useful approach to describe the elastic scattering for p-nucleus at intermediate energies and to investigate the properties of the target nucleus.

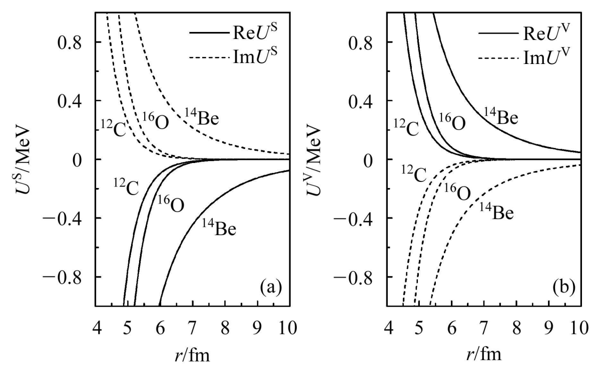

Fig. 1. The Dirac optical potentials, U^{S} (a) and U^{V} (b), of the elastic scatterings for p-^{12}C, p-^{16}O and p-^{14}Be at $E_{\mathrm{lab}} = 800$MeV. The solid lines and the dashed lines represent the real part and the imaginary part of the scalar and the vector potentials, respectively.

The corresponding figures for very small angle behaviors are also presented in Figs. 2—4. From Fig. 2, we note that the positions of the first minimum of $\sigma/\sigma_{\mathrm{M}}$ for the p-^{14}Be, p-^{16}O and p-^{12}C processes appear at angles in an ascending order, and the order will keep unchanged with different incident energies. These phenomena are probably due to the influence of the extended matter distribution, the halo, in ^{14}Be. In Fig. 3 and Fig. 4 we find that in the very small angular region, the values of the spin-related observables A_y and Q in the p-^{14}Be process are larger than those in the p-^{16}O and p-^{12}C processes no matter what incident energy is. These unique phenomena could be explained by the fact that the spin-dependent interaction between the projectile and the target more likely appears in p-^{14}Be than in p-^{16}O and p-^{12}C in the small angular region. Because A_y and Q are spin observables that reflect the spin-dependent NN interaction and are much more sensitive to the target structure,

Table 1. Average Binding Energies (E/A) in MeV, rms Radii ($R_{\rm m}$) in fm and Charge ($R_{\rm ch}$) in fm for ^{16}O, ^{12}C and ^{14}Be.

	^{16}O(Theo.)	^{16}O(Expt.)	^{12}C(Theo.)	^{12}C(Expt.)	^{14}Be(Theo.)	^{14}Be(Expt.)
E/A	−7.733	−7.976(0)	−7.049	−7.680(0)	−4.906	−4.994(9)
$R_{\rm m}$	2.594	2.54(2)	2.35	2.35(22)	3.34	3.20(30)
$R_{\rm ch}$	2.7315	2.7013(55)	2.4986	2.4703(22)	2.4645	2.5036(232)

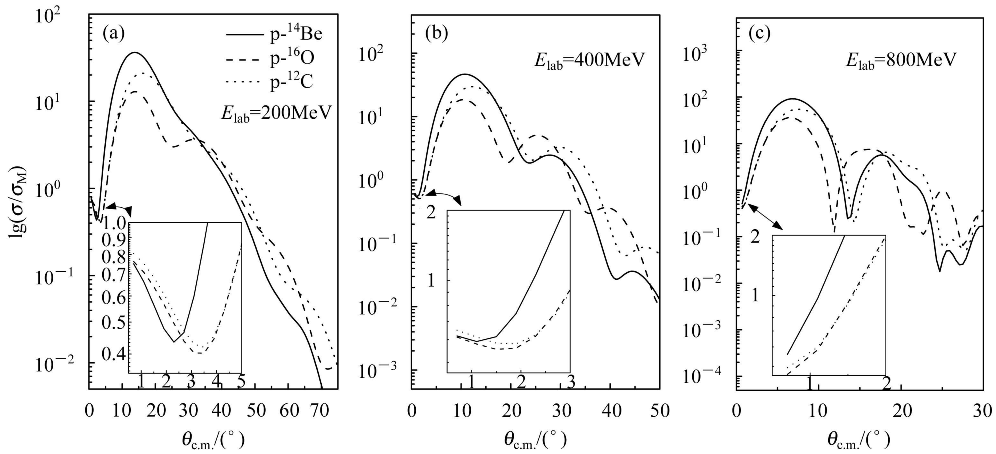

Fig. 2. The $\sigma/\sigma_{\rm M}$ of the elastic scatterings for p-^{12}C (dot), p-^{16}O (dash) and p-^{14}Be (solid) at $E_{\rm lab}=200$MeV (a), 400MeV (b) and 800MeV (c), respectively.

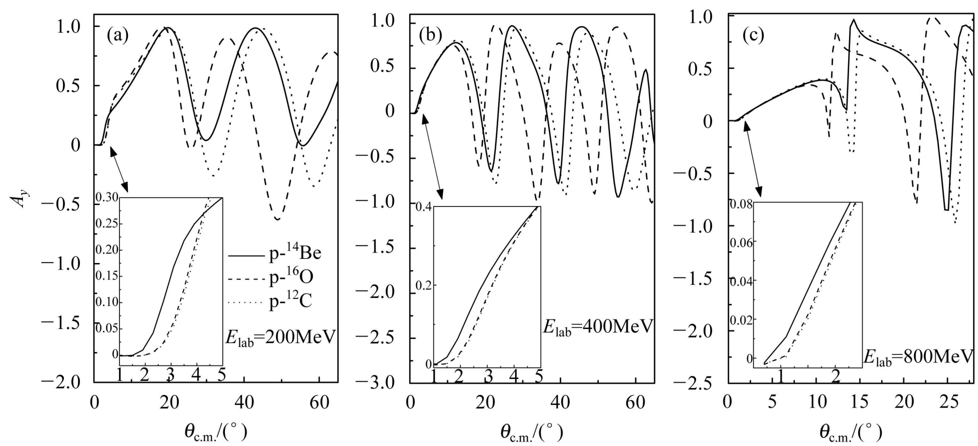

Fig. 3. The same as Fig. 2 but for A_y.

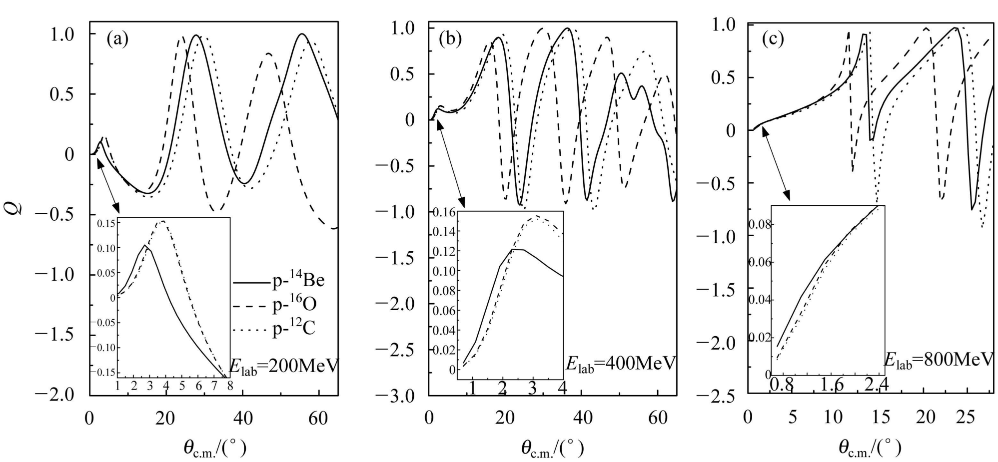

Fig. 4. The same as Fig. 2 but for Q.

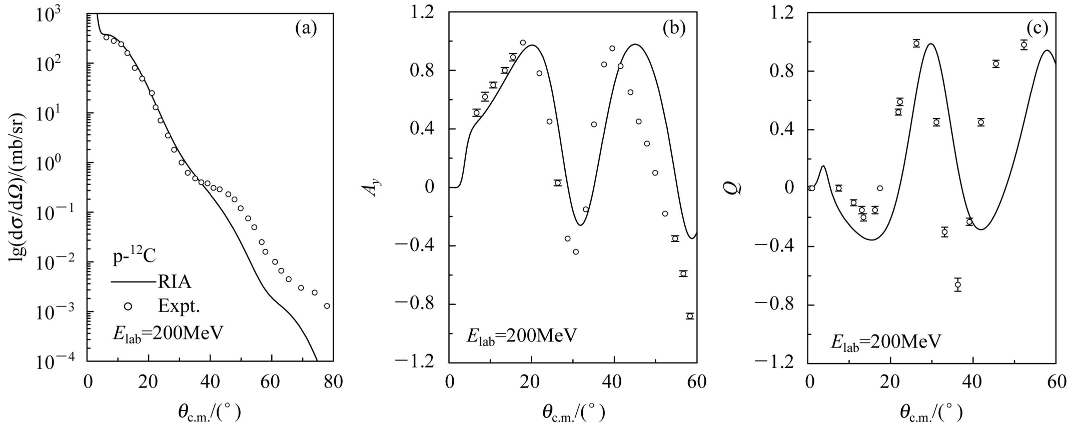

Fig. 5. The observables, $d\sigma/d\Omega$ (a), A_y (b) and Q (c), of the elastic scatterings for p-^{12}C (solid) at $E_{lab} = 200$MeV. The data (circles) are taken from Ref. [28].

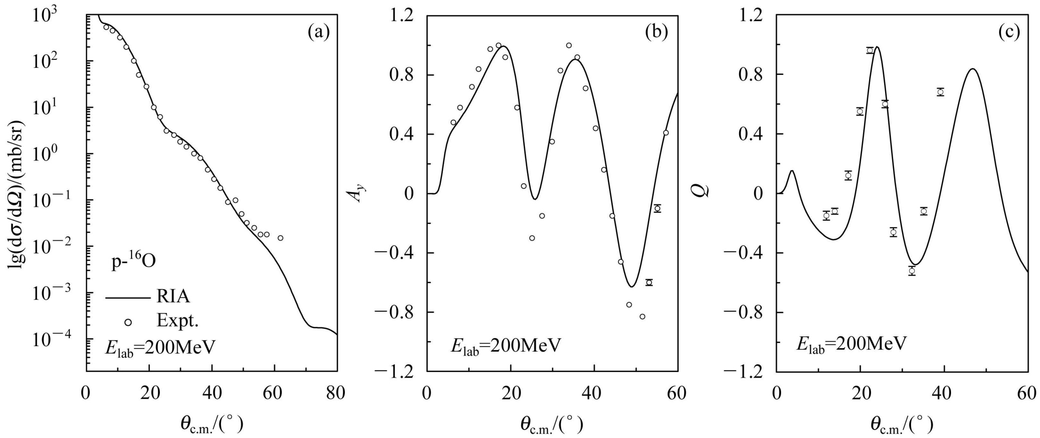

Fig. 6. The same as Fig. 5 but for p-^{16}O (solid).

especially to the nucleon distributions in the target[43], we could use A_y and Q, in addition to σ, of the proton elastic scattering at intermediate energies as two new probes to study halo nuclei.

4 Summary

Based on the RIA formalism, we investigate the elastic scattering observables $d\sigma/d\Omega$, A_y and Q for the exotic system p-^{14}Be, as well as two normal systems p-^{12}C and p-^{16}O, at the intermediate energies $E_{lab} = 200$, 400 and 800MeV, respectively. We find that at different intermediate energies, $d\sigma/d\Omega$, A_y and Q behave consistently, namely the positions of the first minimum of σ/σ_M appear at the angles in an ascending order for the p-^{14}Be, p-^{16}O and p-^{12}C, and the values of the spin-related observables A_y and Q in the p-^{14}Be process are larger than those in the p-^{16}O and p-^{12}C processes. Therefore, in comparison with those in the p-^{16}O and p-^{12}C processes, the behaviors of the differential cross section, the analyzing power and the spin rotation function in the p-^{14}Be process in the small angular region exhibit an unchanged tendency with the variation of the incident energy in the intermediate energy region and the values of $d\sigma/d\Omega$, A_y and Q in the elastic scattering process in the intermediate energy region could be used to investigate the properties of neutron-riched nuclei.

References

1 Hansen P G, Tostevin J. Annu. Rev. Nucl. Part. Sci., 2003, **53**: 219—261

2 Tanihata I, Hamagaki H, Hashimoto O et al. Phys. Rev. Lett., 1985, **55**: 2676—2679

3 Mittig W, Chouvel J M, ZHAN W L et al. Phys. Rev. Lett., 1987, **59**: 1889—1891

4 Zhukov M V, Fedorov D V, Bang J M. Phys. Rep., 1993, **231**: 151—199

5 REN Z Z, XU G O, CHEN B Q et al. Phys. Lett., 1995, **B351**: 11—17
6 PANG D Y, YE Y L, JIANG D X et al. Chin. Phys. Lett., 2004, **21**: 2151—2154
7 Suzuki T, Kanungo R, Bochkarev O et al. Nucl. Phys., 1999, **A658**: 313—326
8 Ozawa A, Bochkarev O, Chulkov L et al. Nucl. Phys., 2001, **A691**: 599—617
9 Neumaier S R, Alkhazov G D, Andronenko M N et al. Nucl. Phys., 2002, **A712**: 247—268
10 Alkhazov G D, Dobrovolsky A V, Egelhof P et al. Nucl. Phys., 2002, **A712**: 269—299
11 LU Z H, WU H Y, HU R J et al. HEP & NP, 2002, **26**(6): 594—599 (in Chinese)
(卢朝晖, 吴和宇, 胡荣江等. 高能物理与核物理, 2002, **26**(6): 594—599)
12 ZHAO Y L, MA Z Y, CHEN B Q. Commun. Theor. Phys., 2003, **40**: 693—698
13 ZHANG S Q, MENG J, ZHOU S G. Sci. Chin. Ser., 2003, **G46**: 632—656
14 REN Z Z, CHEN B Q, MA Z Y et al. Phys. Rev., 1996, **C53**: R572—R575
15 REN Z Z, Faessler A, Bobyk A. Phys. Rev., 1998, **C57**: 2752—2755
16 Navin A, Bazin D, Brown B A et al. Phys. Rev. Lett., 1998, **81**: 5089—5092
17 REN Z Z, Mittig W, Sarazin F. Nucl. Phys., 1999, **A652**: 250—270
18 CAI X Z, ZHANG H Y, SHEN W Q et al. Phys. Rev., 2002, **C65**: 024610
19 WANG Z, REN Z Z. Phys. Rev. 2004, **C70**: 034303
20 Abu-Ibrahim B, Suzuki Y. Phys. Rev., 2004, **C70**: 011603(R)
21 Kobayashi T, Yamakawa O, Omata K et al. Phys. Rev. Lett., 1988, **60**: 2599—2602
22 Dobrovolsky A V, Alkhazov G D, Andronenko M N et al. Nucl. Phys., 2006, **A766**: 1—24
23 Amos K, Richter W A, Karataglidis S et al. Phys. Rev. Lett., 2006, **96**: 032503
24 McNeil J A, Shepard J R, Wallace S J. Phys. Rev. Lett., 1983, **50**: 1439—1442
25 Shepard J R, McNeil J A, Wallace S J. Phys. Rev. Lett., 1983, **50**: 1443—1446
26 McNeil J A, Ray L, Wallace S J. Phys. Rev., 1983, **C27**: 2123—2132
27 Horowitz C J. Phys. Rev., 1985, **C31**: 1340—1348
28 Murdock D P, Horowitz C J. Phys. Rev., 1987, **C35**: 1442—1462
29 Ray L. Phys. Rev., 1993, **C47**: 2990—2993
30 Sakaguchi H, Takeda H, Toyama S et al. Phys. Rev., 1998, **C57**: 1749—1755
31 Baldini-Neto E, Carlson B V, Rego R A et al. Nucl. Phys., 2003, **A724**: 345—353
32 Fergerson R W, Barlett M L, Hoffmann G W et al. Phys. Rev., 1986, **C33**: 239—246
33 GU B P, REN Z Z. Commun. Theor. Phys., 2005, **44**: 337—342
34 Bjorken J D, Drell S D. Relativistic Quantum Mechanics. New York: McGraw-Hill, 1964. 6—18
35 Brieva F A, Rook J R. Nucl. Phys., 1977, **A291**: 317—341
36 Walecka J D. Ann. Phys., 1974, **83**: 491—529
37 Horowitz C J, Serot B D. Nucl. Phys., 1981, **A368**: 503—528
38 CAO L G, MA Z Y. Chin. Phys. Lett., 2004, **21**: 810—812
39 Audi G, Wapstra A H, Thibault C. Nucl. Phys., 2003, **A729**: 337—376
40 Ozawa A, Suzuki T, Tanihata I. Nucl. Phys. 2001, **A693**: 32—62
41 Angeli I. At. Data Nucl. Data Tables, 2004, **87**: 185—206
42 Mott N F, Massey H S W. The Theory of Atomic Collisions. London: Oxford, 1949. 80—87
43 Yoshimura M, Nakamura M, Akimune H et al. Phys. Rev., 2001, **C63**: 034618

入射质子的能量对质子与晕核弹性散射观测量的影响*

顾柏平[1,2;1)]　毛英臣[1]

1 (南京大学物理系　南京　210008)

2 (南京中医药大学数理系　南京　210029)

摘要　用相对论脉冲近似(RIA)对不同的中能质子(200MeV, 400MeV和800MeV)与^{14}Be, ^{16}O和^{12}C的弹性散射进行了研究, 讨论了不同的入射能量对3种观测量, 即微分散射截面、分析本领和自旋转动函数的影响. 研究发现在小散射角的区域晕中子对观察量的影响趋势保持一致, 不随入射质子能量的改变而改变.

关键词　质子弹性散射　相对论脉冲近似　晕核　微分散射截面　分析本领　自旋旋转函数

2006 – 08 – 02 收稿, 2007 – 01 – 29 收修改稿

∗国家自然科学基金(10535010, 10125521), 国家重点基础研究发展规划项目(G2000077400), 中国科学院知识创新工程重大项目(KJCX2-SW-N02)和国家教育部博士点专项基金(20010284036)资助

1) E-mail: medphystcm@126.com